INSTITUTE OF PHYSICS PUBLISHING JOURNAL OF PHYSICS: CONDENSED MATTER

J. Phys.: Condens. Matter **16** (2004) S471–S496 PII: S0953-8984(04)69957-7

Recent advances in nanomagnetism and spin electronics

J F Bobo[1], **L Gabillet**[1] **and M Bibes**[2]

[1] LPMC, FRE 2686 CNRS, 135 avenue de Rangueil, Toulouse Cedex 4, France
[2] Unité Mixte de Physique UMR 137 CNRS-Thales, Domaine de Corbeville, 91404 Orsay, France

Received 30 September 2003
Published 23 January 2004
Online at stacks.iop.org/JPhysCM/16/S471 (DOI: 10.1088/0953-8984/16/5/008)

Abstract

This paper presents recent experimental advances in the field of nanomagnetism and spin electronics. It covers the period of the last decades during which fundamental discoveries such as giant magnetoresistance have been successfully transferred to industrial applications. Such results could be obtained thanks to the improvements of thin film deposition and lithography techniques. Present preparation efforts are now oriented towards lateral size reduction of continuous layers in order to minimize the size of potential devices, as well as to understand better the basic mechanisms of magnetic interactions. At the same time, experimental techniques such as magneto-optic microscopy, magnetic force microscopy, polarized photoelectron spectroscopies or magnetotransport have accomplished significant progress, allowing us to observe in detail magnetic configurations of nanostructures and their magnetoresistive response.

1. Introduction

At the present time, much progress accomplished in sensor technology (for the automotive industry for instance) or data storage (hard drives) is based on discoveries of novel properties of magnetic films, multilayers and micro- or nanostructures. All these results are in the field of nanomagnetism and spin electronics, research domains focused on the study of systems based on heterostructures composed of ferromagnetic (F), antiferromagnetic (AF) and non-magnetic (NM), either metallic or insulating regions. The present paper reviews some of the recent progress made in fundamental physics in this field.

2. Nanomagnetism

In this section, we will focus on nanoscale films and structures, either obtained by the growth on specific substrates or by high resolution electron beam or focused ion beam (FIB) lithography techniques. First, some of the basic concepts of magnetism of ultrathin films will be recalled

for pedagogic purposes, then, recent progress in magnetism of ultrathin films, nanostructures and interactions between F layers separated by NM spacers or exchange coupled to AF films. Several basic papers or book chapters are pertinent references for this section [1, 2].

2.1. Magnetism of ultrathin films and nanostructures

2.1.1. Basic concepts and early results. Thin films are generally of thicknesses of a few atomic planes and one can imagine that, in such a situation, most atoms occupy interface locations and that the small number of atomic planes induces discrete effects. The main issues to be treated are then the conditions of existence of F order and magnetic anisotropy.

A ferromagnetic material can be described in terms of localized magnetism (for example for rare earths) or band magnetism (for transition metals). Thermal stability of F order, in both cases, is related to the perturbation that magnons (spin waves) cause to the zero-temperature F configuration of the system. Below its Curie temperature (T_C), the magnetization decrease from $T = 0$ to finite temperature T is

$$-\Delta M(T)/M(0) = \frac{M(0) - M(T)}{M(0)} = \int \frac{N(E)\,\mathrm{d}E}{\exp(E/k_B T) - 1}. \tag{1}$$

In this expression, $N(E)$ is the magnon density of states (DOS). In the case of isotropic F material, $N(E)$ is proportional to $E^{1/2}$ in 3D (bulk material) and constant in 2D (ultrathin film). In these two cases, the integration of equation (1) will give respectively

(i) in 3D $-\Delta M(T)/M(0) \propto T^{3/2}$ and
(ii) in 2D $-\Delta M(T)/M(0) \propto \infty$.

These thermal dependences predict the existence of F order with a finite $T^{3/2}$ magnetization decrease in 3D and the non-existence of F order for ultrathin films. However, it is possible to add corrective terms to the dispersion of magnons that affect the expression of their DOS and allow some stability of F order in 2D. These terms are either due to finite size effects, anisotropy or dipolar interactions. In the 2D case with perpendicular anisotropy, the system corresponds to the so-called Ising model with a stability of F order and $-\Delta M(T)/M(0) \propto T$.

In contrast to the above mentioned Curie temperature decrease, the $T = 0$ K value of the saturation magnetization of a ultrathin film can be higher than that of the bulk. The following points explain this issue.

(i) Moment can be increased, in the case of itinerant F, due to the coordination decrease z in a ultrathin film. In that case, the 3d band that carries the magnetic moment gets narrower and tends to the bandstructure of a free atom. The DOS at the Fermi level $n(E_F)$ is then increased. The Stoner criterion gives the condition for F order in an itinerant ferromagnet (with I, the repulsive interaction between opposite spin electrons inside the atom):

$$In(E_F) > 1. \tag{2}$$

Since the bandwidth depends on the number of first neighbours and $n(E_F)$ increases when bandwidth decreases, the Stoner criterion is then strengthened, as well as the magnetization. However, the Stoner criterion is not accurate enough to describe all experimental cases; in particular, it does not account for peaks in the DOS that may be present at the Fermi level, due to surface states for instance.

(ii) Epitaxial strain can also cause an increase of the moment due to tensile strain. If tensile strain is not compensated by relaxation in the growth direction, it leads to a larger unit cell volume. In the case of metallic films, this unit cell volume enhancement has the same effect as the reduced coordination at surfaces or interfaces.

(iii) Other effects are in competition with the above mentioned points. For instance, at the NM–F interface, hybridization of the bandstructures either leads to the presence of magnetically dead layers in the F film or induces ferromagnetic polarization to the NM layer (the case for Co grown on Pt, Pd or for Fe on V). Such phenomena are generally difficult to evidence and separate, except by element-sensitive probes such as Mössbauer spectroscopy.

In summary, one can expect a decrease of the Curie temperature and, depending on the unit cell volume change or interfacial hybridization, increase or decrease of the saturation moment for an ultrathin ferromagnetic film.

2.1.2. Ultrathin films. Measurements of low magnetic moments as in ultrathin films are challenging; for example, the magnetization of one monolayer (∼2 Å) of cobalt on an area of 0.1 cm^2 is as low as 3×10^{-6} emu, therefore comparable with the magnetic signal of the substrate. Several solutions exist to solve this problem; the first one is to grow multilayers. In that case, the small amount of magnetic material of the thin film is compensated by the multiplicity of these layers. But then eventual interlayer coupling effects, such as presented in section 2.2.2, have to be accounted for. Interfacial effects also have to be considered, the behaviour of a 'free' ultrathin film (uncovered) being in certain cases different from that of a buried film. Some examples of early results in this field are the observation by *in situ* magneto-optics of the decrease of Curie temperatures of Co on Cu(001) by Bruno [3]. This behaviour could be successfully described taking into account anisotropy and dipolar effects for the Co layer. In the case of Fe–Ru and Fe–Ir superlattices, Piecuch *et al* [4, 5] evidenced the presence of iron magnetically dead layers that they assumed to be due to hybridization of Fe 3d states with the 4d or 5d ones of Ru and Ir. The influence of capping layers was evidenced by Bergter *et al* [6] in the case of Re–Ni bilayers covered by various thicknesses of copper. The Curie temperature of the Ni (10 Å) film was reduced by 80% after only 3–4 Å copper was deposited on its surface.

2.1.3. Magnetic anisotropy. In bulk single-crystal ferromagnets, the intrinsic contribution to anisotropy is related to the crystal structure of the material. It is called the magnetocrystalline anisotropy and is generally weak (10^{-3}–10^{-6} eV/atom). Its origin is the rotational invariance breakdown caused by spin–orbit coupling. This bulk anisotropy K_v is phenomenologically developed along the crystallographic main axes of the crystal. So cubic structures have a fourfold magnetocrystalline anisotropy (iron or nickel for example) while hexagonal ones (hcp cobalt) have a twofold one along the c axis and sixfold in the a–b plane [1]. Note that specific alloys such as permalloy ($Ni_{80}Fe_{20}$) have extremely weak magnetocrystalline anisotropy and are commonly used for low field sensors. In the case of thin films, demagnetizing field effects are dominant. These effects appear when magnetic flux lines come out of the surface of a F body, i.e. when the magnetization is not exactly in the plane of a thin F film, for instance. The magnetostatic energy (demagnetizing or shape anisotropy) expression, in the case of a uniformly magnetized (M_S) thin film, its magnetization making an angle θ with respect to the plane of the film, is

$$E_D = -2\pi M_S^2 \sin^2\theta. \tag{3}$$

Equation (3) is valid for an infinitely extended flat film. Roughness or finite size effects may affect this expression. The use of ultrathin films or nanostructures gives rise to other anisotropy terms that may overcome magnetocrystalline or demagnetizing field effects. One of the most significant anisotropy terms appearing in ultrathin films is *interface anisotropy*. In a ultrathin film, interface atoms are subjected to strong anisotropy fields either caused by

symmetry breakdown or large strain accumulation due to epitaxial growth. The resulting anisotropy, K_i, adds to the total effective anisotropy K_{eff}:

$$K_{\text{eff}} = \frac{2K_i}{t_{\text{F}}} + K_{\text{v}} - 2\pi {M_{\text{S}}}^2. \tag{4}$$

In equation (4), t_{F} and M_{S} are respectively the thickness and saturation magnetization of the F ultrathin film. The factor of two in the first term accounts for both interfaces of the film. This is valid if they are identical. The first observation of interface anisotropy in transition metal systems was made by Gradmann and Müler [7]. Since then, numerous studies have evidenced compatible transition metal systems for stabilizing perpendicular anisotropy in ultrathin F films, e.g. Pt–Co–Pt [8], Pd–Co–Pd or Au–Co–Au sandwiches. Thermal stability of perpendicular anisotropy was also studied by *in situ* magneto-optics for the Fe–Cu system [9].

2.1.4. Nanostructures. Most of the recent advances in nanomagnetism were made in the field of laterally structured magnetic thin films. Two main categories can be distinguished. The first one concerns the growth of thin films on nanostructured substrates (step-bunched or nanofaceted); the second one concerns thin film patterning by lithography or nanolithography techniques.

In the first category, important efforts have been made to investigate the magnetic properties of iron films deposited on single-crystal tungsten substrates. More precisely, Elmers *et al* [10, 11] used stepped W(110) single crystals to evidence the unusual magnetic properties of iron nanostripes. Combined use of Kerr magnetometry and *in situ* spin-polarized tunnelling microscopy (SP-STM) helped them to observe the one-dimensional magnetic configuration in the system. They could generate, in partially magnetically reversed magnetized states, extremely narrow domain walls (DWs) as thin as 6 Å (see the SP-STM image of figure 1). This yields a value for the exchange stiffness constant of iron far below that of the bulk in ultrathin film (1.8×10^{-12} J m^{-1} for Fe nanostripes versus $1–2 \times 10^{-11}$ J m^{-1} for bulk Fe). This kind of result emphasizes the important changes of magnetic properties of low dimensional systems compared to those of the bulk.

Dubourg *et al* [12] have demonstrated the possibility of growing high quality epitaxial nanofaceted nickel oxide by reactive sputtering on MgO(110). The nanofaceted morphology of NiO(110) is obtained thanks to the large atomic plane energy difference between (100) and (110) planes that favours spontaneous decomposition of the nominal (110) NiO surface into elongated (100) nanofacets. The growth of Co on top of such a surface either leads to continuous films with conformal morphology in the case of sputtering, or to the formation of nanowires or aligned nanocrystals for evaporated Co layers [13]. This discontinuous metallic film growth in valleys of nanogrooved surfaces was initially studied by Sugawara *et al* [14] and is a promising way for obtaining nanowires without the lithography technique. The magnetic properties of such nanostructures reveal either paramagnetic or slightly ferromagnetic behaviour at room temperature for nanowires or isotropic exchange-biased ferromagnetic behaviour for the nanocrystal rows as shown in figure 2.

In the second category, investigators use either electron-beam (e-beam) or FIB lithography techniques to pattern continuous layers. A recent review in this field was done by Martín *et al* [15]. Some remarkable results detailed here concern submicronic permalloy ($Ni_{80}Fe_{20}$) dots in dipolar interaction by Cowburn and Welland [16–19]. He was the first to validate the feasibility of *Nanomagnetic Logic Devices*. In the particular case of elliptic dots presented in figure 3, due to stray field coupling between two consecutive dots, synthetic antiferromagnetic order could be generated and evidenced by high resolution Kerr magnetometry. The magnetization

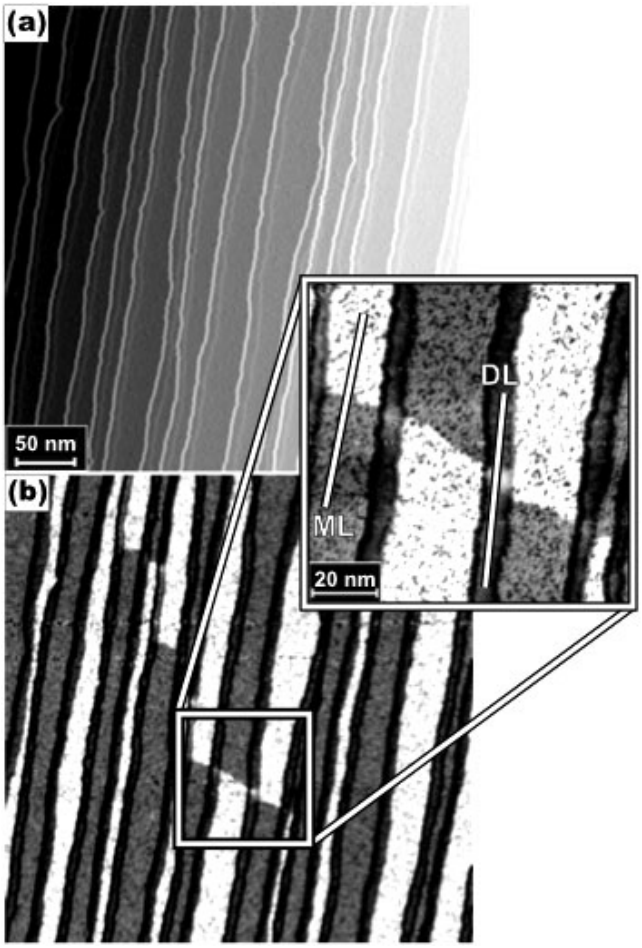

Figure 1. STM (a) and SP-STM (b) images of the surface of iron nanostripes deposited on a W(110) stepped single crystal. The spin-resolved images evidence the presence of DWs as thin as 6 Å. Courtesy [10].

easy axis within each dot is perpendicular to the row line due to shape anisotropy designed by patterning.

Dipolar interaction between micro/submicronic patterned arrays can also be evidenced by imaging techniques such as Kerr microscopy. In this domain, Hrabovský *et al* [20] observed collective magnetic switching of iron square-shaped dots of micrometric size separated by submicron gaps (see figure 4).

Another original way to obtain patterned dots in interaction was used by FIB localized irradiation of Pt–Co–Pt sandwiches by Hyndman *et al* [21–24]. Ga ion irradiation causes atomic displacements and some intermixing in the Co layer and its interfaces with Pt. The consequence is a reduction of the Curie temperature and anisotropy of the alloy and therefore the presence of F areas (not irradiated) in contact with paramagnetic zones that received the ion beam. That technique causes no morphological changes to the films but allows a modulation of its magnetic properties. The resolution of the technique is better than 200 Å. So these authors could observe, as shown in figure 5, ordered arrays of successively up and down magnetized dots due to the dipolar interaction between neighbour squares.

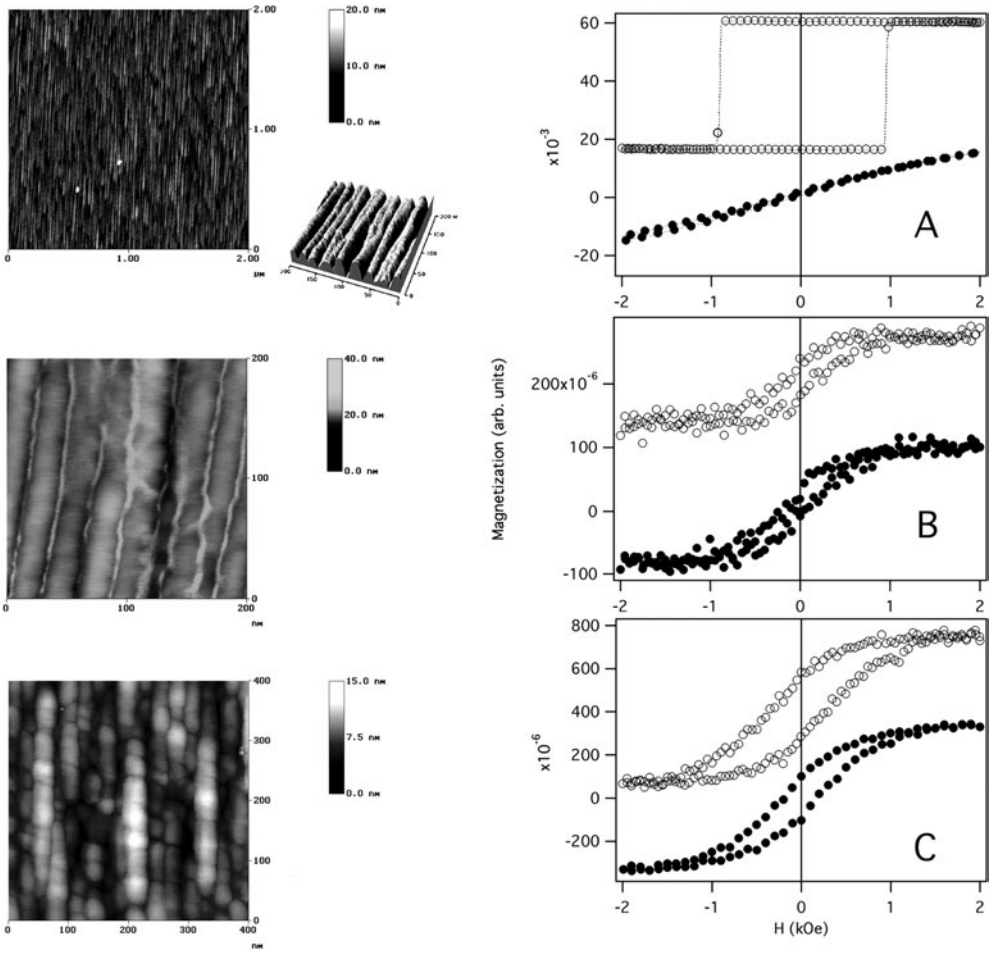

Figure 2. Atomic force microscopy images of NiO–Co surfaces in the cases of a continuous layer (A), nanowires (B) and nanocrystals (C). In sample A, the Co layer uniformly covers the NiO surface. In sample B, the faint bright lines located in the valleys of NiO are Co nanowires. Finally, for sample C, Co nanocrystals are aligned along the NiO nanofacets. Room temperature hysteresis loops along the NiO nanofacets (open circles) and perpendicular (black circles) in these three cases are shown on the right.

2.2. Couplings

2.2.1. Magnetic coupling between a ferromagnet and an antiferromagnet. The magnetic interaction across the interface between a ferromagnetic spin system and an antiferromagnetic spin system is named exchange coupling. This interaction was first discovered in 1956 by Meiklejohn and Bean [25–28] when studying Co particles embedded in their native antiferromagnetic oxide (CoO). Since then, it has been observed in many different systems containing F–AF interfaces such as small particles, inhomogeneous materials, F films on AF crystals and thin films.

Phenomenology. The general phenomenological features of this anisotropic exchange coupling are a shifted hysteresis loop and/or an enhancement of the coercivity, a $\sin\theta$ torque curve, and a high field rotational hysteresis.

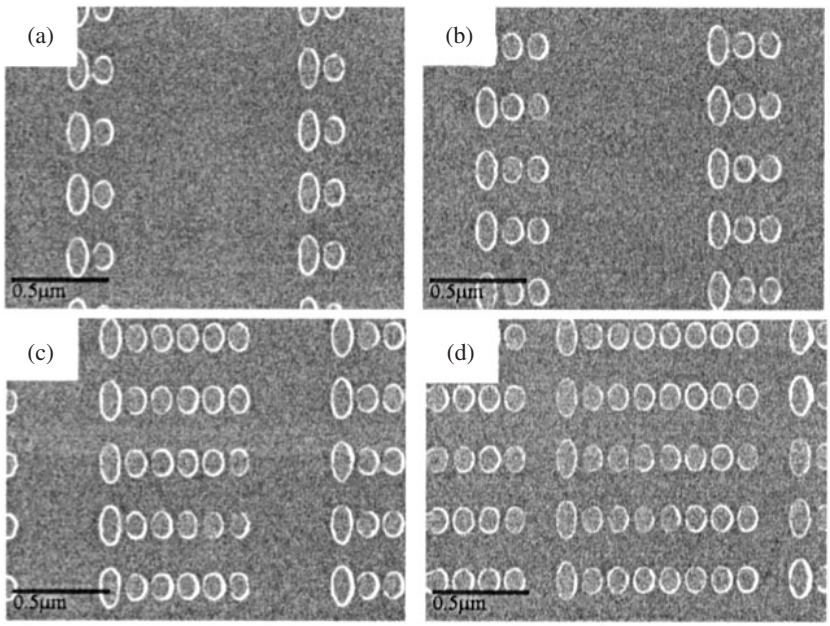

Figure 3. Permalloy nanodot rows with various dot numbers and elliptic shape in order to observe antiparallel configuration. Courtesy [18].

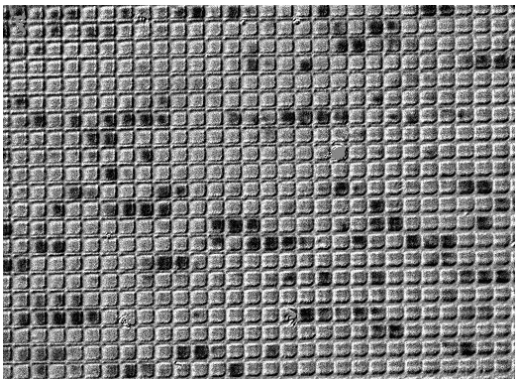

Figure 4. High resolution Kerr image of an iron (400 Å thick) square lattice (square size = 3.5 μm, spacing = 0.5 μm) during its magnetic switching. The applied field is horizontal and one can observe rows of several squares switching collectively thanks to dipolar coupling. Courtesy [20].

The hysteresis loop shift, generally known as exchange bias, H_E, is usually observed after cooling the AF–F couple through the Néel temperature (T_N) of the AF in the presence of an external magnetic field. The Curie temperature (T_C) of the F must be greater than the Néel temperature of the AF and the initial temperature must be above T_N, but below T_C in order to saturate the magnetization of the F. The hysteresis loop of the system at $T < T_N$ is displaced along the field axis generally in the opposite (negative) direction to the cooling field, leading to different absolute values of coercive field for decreasing and increasing field. The hysteresis loops also have an increased coercivity, H_C, after the field cool procedure.

Torque magnetometry at $T < T_N$ after field cool shows an additional $\sin\theta$ component to the torque magnetization, where θ is the angle between the applied magnetic field and

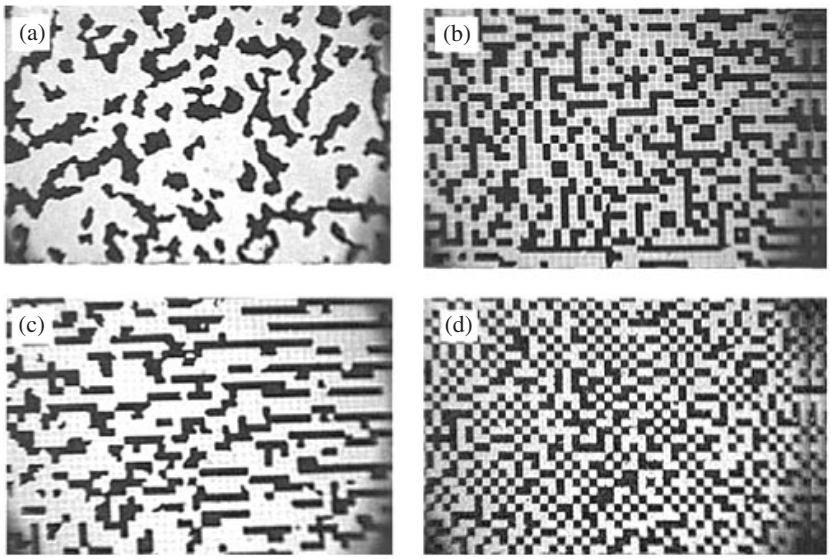

Figure 5. Typical domain patterns of array of FIB-irradiated Pt–Co–Pt trilayers (square mesh of 3 μm) observed by Kerr microscopy. The image area is $150 \times 100\ \mu\text{m}^2$. Various Ga irradiation fluences f reveal patterns characteristic of continuous films ((a) $f = 2 \times 10^{13}$ ion cm^{-2}). Courtesy [22].

the cooling field direction. The $\sin\theta$ torque function indicates that exchange anisotropy is a unidirectional anisotropy and not a uniaxial anisotropy as represented by a $\sin^2\theta$ torque function. The clockwise and anticlockwise torques are different. The area between both torque curves gives twice the energy lost in rotating the magnetization, denoted as rotational hysteresis.

All these effects vanish above a temperature often denoted as the blocking temperature T_B. For systems with very thin films, T_B is much lower than the bulk T_N; however, single-crystal AF and thick AF films with large grains tend to have $T_B \approx T_N$, confirming that the presence of the AF material is the origin of this anisotropy. This low T_B value may be attributed to a T_N decrease of the thin AF film, as is the case for ultrathin F films (see section 2.1.1).

Origin of the unidirectional anisotropy. Exchange bias can be qualitatively understood by assuming an exchange interaction at the AF–F interface. When a field is applied in the temperature range $T_N < T < T_C$, the F spins line up with the field, while the AF spins remain random. As the material is cooled through T_N, in the presence of the field, due to the interaction at the interface, the AF spins next to the F align ferromagnetically to the latter (assuming ferromagnetic interaction). The other spin planes in the AF 'follow' the AF order so as to produce zero net magnetization. When the field is reversed, the F spins start to rotate. However, for sufficiently large AF anisotropy, the AF spins remain unchanged and exert a microscopic torque on the F spins, to keep them in their original position (ferromagnetically aligned with the AF spins at the interface). Since the AF spins hold the F spins in the field cooling direction (single stable configuration), the anisotropy is unidirectional. Thus, the field needed to reverse completely a F layer will be larger if it is in contact with an AF, because an extra field is needed to overcome the microscopic torque (larger H_C). However, once the field is rotated back to its original direction, the F spins will start to rotate at a smaller field,

due to the interaction with the AF spins (which now exert a torque in the same direction as the applied field). The material behaves as if there were an extra (internal) biasing field; therefore, the F hysteresis loop is shifted in the field axis.

In this intuitive model, the energy per unit area of an exchange bias system can be written as

$$E = -H M_{\mathrm{F}} t_{\mathrm{F}} \cos(\theta - \beta) + K_{\mathrm{AF}} t_{\mathrm{AF}} \sin^2 \alpha - J_{\mathrm{INT}} \cos(\beta - \alpha) \tag{5}$$

where H is the applied field, M_{F} the saturation magnetization, t_{AF} the thickness of the AF layer, K_{AF} its anisotropy and J_{INT} the interface coupling constant. β, α and θ are respectively the angles between the magnetization (M_{F}) and the F anisotropy axis, the AF sublattice magnetization (M_{AF}) and the AF anisotropy axis, and the applied field and the F anisotropy axis. This model assumes coherent rotation of the magnetization, collinear AF and F anisotropy axes, negligible F anisotropy and ferromagnetic coupling at the interface. The first term in the energy equation accounts for the effect of the applied field on the F layer (Zeeman term), the second term takes into account the AF anisotropy and the last term takes into consideration the interface coupling. Minimizing the energy with respect to α and β, the loop shift is found to be [28]

$$H_{\mathrm{E}} = \frac{J_{\mathrm{INT}}}{M_{\mathrm{F}} t_{\mathrm{F}}}. \tag{6}$$

Another important result from this minimization is that the condition $K_{\mathrm{AF}} t_{\mathrm{AF}} \geqslant J_{\mathrm{INT}}$ is required for the observation of exchange anisotropy. If the above condition is not satisfied, the AF spins follow the motion of the F layer, thus no loop shift should be observed but only an increase in coercivity [28].

The exchange bias magnitude predicted by these previous calculations depends on the assumed value for J_{INT}. If J_{INT} is taken to be similar to the ferromagnetic exchange, H_{E} is predicted to be several orders of magnitude larger than the experimental results. This discrepancy can be explained by considering the spin configuration at the interface. Two main issues concerning the orientation have been addressed: compensated (zero surface magnetization) versus uncompensated (non-zero surface magnetization) AF surfaces and in-plane versus out-of-plane AF spins. Intuitively, one may expect that, for compensated surfaces, the spins pinning the F cancel, giving rise to a net zero H_{E}. However, it was found that all compensated surfaces experimentally investigated exhibit exchange bias, often larger than uncompensated orientations of the same AF materials. This effect could be due to the formation of domains in the AF layer, non-collinear (or perpendicular) coupling at the interface, spin wave transfer between the F and the AF layer or residual uncompensated spins at the interface. Usually, the theories assume that the AF spins at the interface lie on the interface plane (e.g. $FeF_2(110)$). However, certain orientations of some AF materials have spins pointing out of the interface plane (e.g. $FeF_2(001)$) [29]. When the AF spins are in the plane, H_{E} is maximum, but when the spins are completely (90°) out of the interface plane $H_{\mathrm{E}} = 0$.

These models have attained different degrees of agreement with existing experimental results. Often the individual approximations apply for a specific system and are not valid for other systems. Clearly, the exchange bias H_{E} depends strongly on the spin structure at the interface (e.g. orientation or interface disorder due to roughness or crystallinity). However, many factors, including the role of F and AF domains or the perpendicular coupling at the interface, are still poorly understood. So, from the basic point of view, there is a need for studies aimed at understanding the interface spin structure, using novel tools such as magnetic dichroism or using conventional ones, such as neutron diffraction or Mössbauer spectroscopy, in unconventional ways.

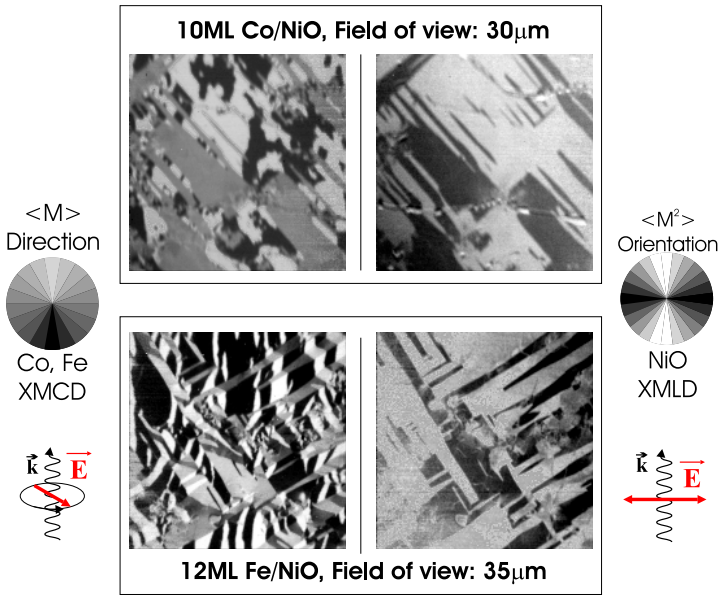

Figure 6. Magnetic domain imaging of NiO–Co and NiO–Fe structures evidencing correlations between the domain structures of AF and F. Courtesy [31].
(This figure is in colour only in the electronic version)

In the case of x-ray magnetic dichroism imaging, a recent study by Ohldag *et al* [30] by x-ray PEEM (photo-emission electron microscopy) has revealed the correlation between the domain structure of the NiO single-crystal AF substrate and the F films deposited on top (either Co or Fe). Circular polarized photons were used to probe the orientation of F domains while linearly polarized photons evidence the orientation of the spins in the AF (see figure 6). This technique is very powerful but requires the use of thin F capping layers due to the low photoelectron mean free path (from 20 to 40 Å).

Origin of the coercive field enhancement. The coercivity usually increases below T_B, which is probably linked to the anisotropy of the AF layer. In the case of an AF with small anisotropy, when the F rotates, it 'drags' the AF spins irreversibly, hence increasing the F coercivity. For a large AF anisotropy, the F decouples because it cannot drag AF spins, consequently the coercivity is reduced. A consequence of the influence of the anisotropy on the coercivity is the peak on the H_C versus T curve which it often exhibits close to T_B. This peak is due to the decrease of AF anisotropy close to T_B. As the anisotropy decreases, the F layer is able to drag increasingly more AF spins, thus increasing the coercivity. Above T_B the AF is random, thus it does not hinder F layer magnetization rotation. The width is related to sample homogeneity. In actual samples, there is some spread on grain sizes, interface couplings, stress and so on, which causes a distribution of AF anisotropies. The distribution of AF anisotropies reflects itself in the coercivity and therefore this peak mimics the sample inhomogeneity.

A similar peak behaviour close to T_B has also been observed in the rotational hysteresis of some systems. This indicates that the coercivity and the rotational hysteresis are different manifestations of the same effect, i.e. the losses produced during the rotation of the F layer by the AF spin drag.

An analogous peak effect is found in the AF thickness dependence of H_C or the rotational hysteresis at a fixed temperature. The explanation of this thickness dependent effect is similar

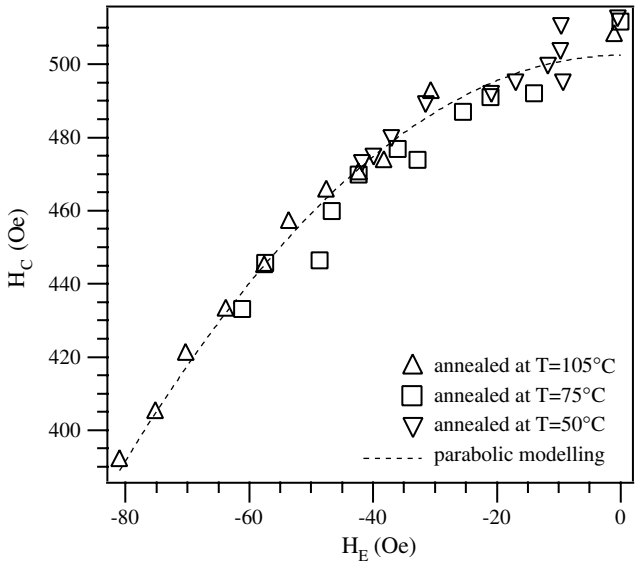

Figure 7. Correlation between H_C and H_E for NiO–Co(110) epitaxial bilayers annealed at various temperatures [32].

to the previous temperature one. In this case, as the AF thickness decreases, the effective AF anisotropy, $K_{AF}t_{AF}$, is reduced. Thus, the F can drag more AF spins as the AF layer becomes thinner, increasing the coercivity. For thin enough films, the AF layer is no longer magnetic, thus it stops hindering the F rotation. However, one cannot rule out other pinning mechanisms, such as inhomogeneities in the AF–F coupling or thermal fluctuations, as the source of these peak effects.

We have recently succeeded observing a clear correlation between H_C and H_E in epitaxial NiO–Co bilayers epitaxially grown on MgO(110) (see section 2.1.4 for structural details). After thermomagnetic treatments of such samples (typically $NiO_{335\,Å}Co_{80\,Å}$), the exchange bias field was increased as expected but the coercive field was simultaneously decreased. The relationship between H_C and H_E shown in figure 7 can be interpreted in terms of magnetic reorganization of the NiO AF layer reducing the number of AF domains in the high H_E state. This effect is not observed in the case of polycrystalline NiO–Co bilayers because the AF domain extension is then limited by the grain size (∼200 Å) in contrast to single-crystal epitaxial NiO films [32].

Influence of several parameters. Exchange bias is roughly inversely proportional to the thickness of the F layers ($H_E \propto 1/t_F$), indicating that it is an interface effect. This relation holds for fairly thick F layers (several thousands of ångströms), as long as the thickness is smaller than the F DW size. However, if the F layer is too thin, the relation is no longer valid, probably because the F layer becomes discontinuous.

The dependence of H_E on the AF thickness is more complicated. The general trend is that for thick AF layers, e.g. over 200 Å, H_E is independent of the thickness of the AF layer. As the AF thickness is reduced, H_E decreases abruptly and finally, for thin enough AF layers (usually a few tens of ångströms), H_E becomes zero. The exact thickness at which the different stages in this process take place depends on the specific system, its microstructure and the measurement temperature.

In many exchange biased film systems, H_E depends on the number of measurements, a property often called the training effect. If several consecutive loops are measured, the shift will decrease. It is often found experimentally that $H_E - H_{E\infty} \propto 1/\sqrt{n}$, where n indicates the order in which consecutive loops are measured. However, it is important to stress that this phenomenon is more important in polycrystalline AF, and very small or non-existent in systems based on single crystals. This effect seems to be related to partial reorientation of the AF domains with each F magnetization reversal. The origin of this effect may lie in a growth induced metastable spin configuration, an induced thermoremanent magnetization in the AF layer, which exhibits some reptation effects, or caused by thermal fluctuations when $K_{AF} v_{AF} < k_B T$ (v_{AF} being the elementary domain volume of the AF). The AF spins try to find energetically favourable configurations after each cycle. Some very recent work on NiO/Co bilayers shows that the bias field has a logarithmic dependence on the time and that the rate of variation is directly connected to the anisotropy of the NiO AF layer which governs the relaxation of non-compensated AF domains at the interface. The characteristic time constant could be as short as 5 min or as long as several days, depending on the sample preparation method [33].

Generally, H_E does not depend markedly on cooling field. However, studies in FeF_2/Fe [34] and MnF_2/Fe [35] bilayers revealed a rather unusual behaviour. For large cooling fields, the loops shift to positive fields, i.e. in the same direction as the cooling field. This effect is often called positive exchange bias. The magnitude of the cooling field needed to obtain a positive shift depends strongly on the microstructure of the sample, and thus the interface coupling at the interface. All theoretical models proposed to explain this effect are based on the existence of an antiferromagnetic coupling at the interface between the F and AF layers.

In a recent work [36], we have investigated the influence of the NiO layer deposition method on the magnetic properties of a AF/F coupled NiO/Co bilayer, forming the hard electrode of our NiO/Co/Al_2O_3/Co magnetic tunnel junction (MTJ). We showed that, depending on the preparation method, it is possible to control the anisotropy and the exchange bias of the NiO/Co bottom electrode. The larger bias field is obtained in samples grown under a 1 kOe magnetic field, whereas the best anisotropic behaviour is obtained by sputtering the NiO with a fixed position of the sample holder inside the facing target magnetron. So, it is possible to impose the dominating mechanism responsible for the exchange coupling (e.g. magnetoelastic effects in the AF layer or magnetic ordering in the F layer) according to the deposition mode.

We have also recently probed an original way for inducing exchange bias in AF–F bilayers by using isothermal intense magnetic field saturation. 550 kOe field pulses were applied at room temperature along in-plane specific directions of FeMn–NiFe or NiO–Co bilayers. This method consists in applying a sufficiently large magnetic field to the AF material so that is passes from AF phase (low field) to paramagnetic or spin-flop phase at strong field. The technique is not based on thermomagnetic treatment with magnetic field cooling. It is fast and prevents sample damage by heating. First results were promising: modification of H_E or H_C values or changes in the in-plane anisotropy axes [37].

Applications. The first proposed application of exchange bias in bilayers was as magnetic recording media. Small areas of an F–AF bilayer were heated up to $T_N < T < T_C$ in the presence of a field opposite to the exchange bias field, thus forming areas with reversed magnetization to the overall magnetization of the film. Another proposed application is as domain stabilizer in recording heads based on anisotropic magnetoresistance. An AF layer is deposited on the edges of the F layer, to avoid closure domains, and thus reduce the Barkhausen noise of the devices. Finally, since the discovery of giant magnetoresistance (GMR) in exchange bias spin valves, a variety of devices have been built and proposed,

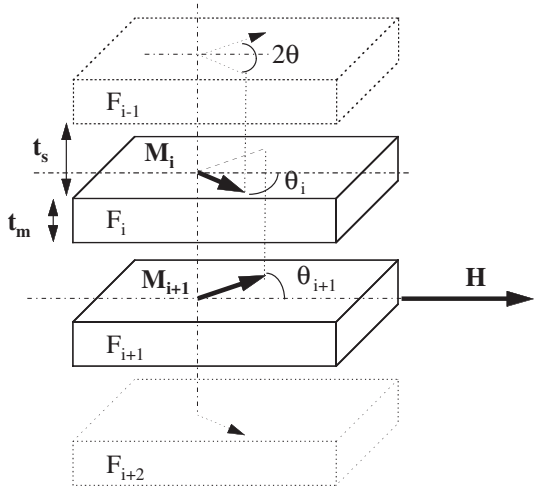

Figure 8. Schematic representation of the bilinear interaction between ferromagnetic layers in a multilayered system.

such as read-heads, magnetic sensors or magnetoresistive memories. The main aims in this application field are to improve the layer quality to develop materials with large H_E, high T_B (well above room temperature), good corrosion resistance and electrical conductivity in the case of current-perpendicular-to-plane (CPP) applications such as MTJs (see section 3.1.2).

For more details and references concerning the exchange anisotropy, you can refer to a recent review by Nogués and Schuller [38].

2.2.2. Interlayer coupling through non-magnetic material. Since the discovery of GMR [43], there has been strong interest in the investigation of coupling between ferromagnetic layers through non-magnetic interlayers. The motivation is to understand the physics of coupling and its effects on the properties and stability of spin-valve structures or MTJs. So far there are various interlayer coupling mechanisms reported and it is primordial to identify and control the effect of each interaction on the magnetic switching characteristics of a multilayer.

A first approach consists in considering a *bilinear* interaction between the ferromagnetic layers (figure 8). This coupling is described as bilinear since the relative surface coupling energy is proportional to the magnetization product

$$E_c = -J\vec{m}_i\vec{m}_{i+1} = -J\cos(\theta_i - \theta_{i+1}) \tag{7}$$

where J is the interaction strength (or coupling constant), $\vec{m}_i$ and $\vec{m}_{i+1}$ are the magnetization unit vectors of two consecutive ferromagnetic layers in a multilayer and θ_i and θ_{i+1} are the magnetization angles measured relative to the applied field direction. According to this equation, a positive interaction strength promotes a parallel alignment, the coupling is said to be ferromagnetic and a negative interaction strength induces an antiparallel alignment; this is called antiferromagnetic coupling.

Generally, the bilinear coupling in spin-valve structures or MTJs results from the combination of two contributions:

(i) the conduction-electron-mediated exchange coupling, which oscillates in sign as a function of the thickness of the metallic spacer layer and which is closely related to the well known RKKY interaction between magnetic impurities, and

(ii) the dipolar magnetic coupling (also known as Néel coupling or 'orange-peel' coupling), which is ferromagnetic and comes from magnetostatic charges present at the interfaces and induced by surface roughness.

We can state precisely that other magnetostatic couplings do exist. The most famous is the antiferromagnetic coupling due to geometric demagnetizing fields (also called stray fields) of ferromagnetic films in patterned systems. This coupling is smaller when decreasing the layer thicknesses and increasing the pattern size. A second kind of magnetostatic coupling is induced by the DW interactions. We will keep in mind the existence of these two couplings but this review will not describe them.

A second coupling contribution was introduced since sandwich structures produced experimentally sometimes show behaviours not accounted for by the bilinear coupling model. These multilayers can exhibit a net magnetic moment in the absence of an external field and a non-linear magnetization curve. A phenomenological way to describe the behaviour is to add a biquadratic term to the energy

$$E_{\mathrm{b}} = -B(\vec{m}_1\vec{m}_2)^2. \tag{8}$$

B is negative and favours perpendicular spin moment alignment at zero field. This coupling may be explained by physical defects, and more particularly by the presence of pinholes, namely ferromagnetic bridges connecting the two ferromagnetic films across the interface.

Oscillatory exchange coupling (RKKY). When ferromagnetic films are separated by a metallic paramagnetic spacer layer, the magnetizations of the layers are coupled to each other by an exchange interaction through the electrons of the spacer layer. As the thickness of the spacer layer is varied, the coupling can oscillate in sign and generally dominates at small spacer layer thickness. This coupling was first observed in 1986, both in transition metal multilayers [39, 40] and in rare-earth multilayers [41, 42]. Shortly thereafter the GMR was discovered in Fe/Cr multilayers [43]. Parkin [44] investigated interlayer coupling between Fe, Co or Ni layers separated by many non-magnetic transition metals and showed that oscillatory interlayer coupling was a rather general feature.

This coupling has essentially the same origin as the oscillatory coupling, known as the RKKY (Rudermann, Kittel, Kasuya and Yosida) interaction [45], between magnetic impurities in a non-magnetic host. In both cases, localized and spin-polarized disturbances, interfaces in one case and impurities in the other are coupled to each other by their influence on the electrons in the spacer or host, respectively.

Early models consider the indirect exchange interaction between two two-dimensional sheets of impurities embedded in a non-magnetic host. From the analytical expression of this interaction in the 2D case (multilayers) and while only considering what occurs along the axis growth (pseudo-1D interaction), it is possible to show that spin polarization and coupling oscillate with a $\Lambda = 2\pi/2k_{\mathrm{F}} = \lambda_{\mathrm{F}}/2$ period [46]. However, experimental investigations on many multilayer systems show Λ_{exp} coupling periods much larger than the half Fermi wavelength of the paramagnetic spacer ($\lambda_{\mathrm{F}}/2 \approx 2$ Å while $\Lambda_{\mathrm{exp}} \approx 10$ Å). This difference was first explained by a Vernier effect between the space lattice parameter and the half Fermi wavelength period [47, 48].

Then, further refinement by Bruno and Chappert [49] emphasized the role of the intrinsic properties of the material that makes up the spacer, namely its Fermi surface. Their theory shows that the periods of the oscillatory coupling are determined by critical spanning vectors of the Fermi surface of the spacer. These vectors are in the direction of the interface normal, that connect two sheets of the Fermi surface that are parallel to each other at the endpoints of

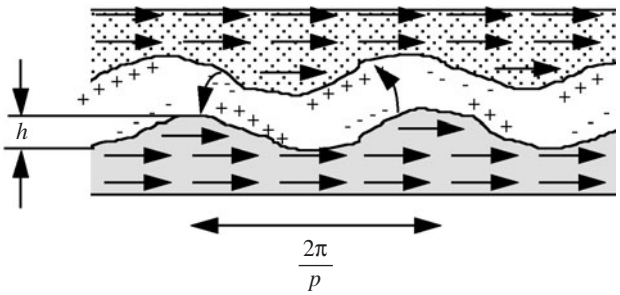

Figure 9. Schematic representation of a trilayer with conformal sinusoidal interface roughness inducing orange-peel F coupling.

the vector. So, the oscillatory periods depend on the topological properties of the spacer Fermi surface and the coupling strength is essentially in $1/t^2$ where t is the interlayer thickness. The coupling constant J is given by equation (9):

$$J(t) = \frac{J_0}{t^2}\sin\left(\frac{2\pi t}{\Lambda} + \Psi\right)\frac{t/\Lambda}{\sinh(t)/\Lambda}. \tag{9}$$

Λ and Ψ are the oscillation period and phase. Moreover, this model predicts that a multiplicity of oscillation periods may be encountered, the number and values of which depend upon the growth direction of the samples. The investigations by Johnson *et al* [50, 51] in epitaxial (100), (111) and (110) Co/Cu/Co sandwiches with wedge-shaped Cu layers supply strong experimental support of this Fermi surface picture. Thus, although RKKY-based models may not use an appropriate description of the magnetism in transition metals, they point out some of the most important general features of models for the interlayer exchange coupling. Bruno's [52] quantum well model was developed in order to take into account the itinerant electrons of the transition metal. His theory describes the non-magnetic spacer as a potential gap for conduction electrons and considers the difference between energy bands of the electrons in the ferromagnetic and in the spacer.

A more detailed review about interlayer exchange coupling has recently been published by Stiles [53].

Magnetostatic (Néel or 'orange-peel') coupling. It was Néel, in 1962 [54, 55], who pointed out that there should be ferromagnetic coupling between adjacent films due to magnetic dipoles at the interface induced by a morphological corrugation. His model describes the magnetostatic interaction between two ferromagnetic layers (free and pinned; saturation magnetizations M_F, M_P) of infinite thickness, separated by a non-magnetic spacer (thickness d) with a correlated interface waviness with amplitude h and wavelength $\lambda = 2\pi/p$ (figure 9). The interlayer coupling constant J is given as [56–58]

$$J = \frac{\pi^2 h^2 \mu_0 M_F M_P}{\lambda\sqrt{2}}\exp\left(-\frac{2\pi d\sqrt{2}}{\lambda}\right). \tag{10}$$

This model predicts an increase of the dipole coupling between the magnetic layers with decreasing spacer thickness. The offset field (Néel field) of the free layer with thickness t_F can generally be expressed as

$$H_N = \frac{J}{\mu_0 M_F t_F}. \tag{11}$$

In 1999, more refined analyses were proposed in order to take into account the finite thickness of the ferromagnetic layers [56, 58]. Indeed, magnetic poles created at the outer surfaces of the magnetic layers result in additional interactions which have to be considered. It has been found that the coupling field increases slightly with the pinned layer thickness and decreases with the free layer thickness. The most important assumptions entering the model are a uniform magnetization within the layers and a correlated roughness, i.e., there is no phase, amplitude or correlation length difference in the topology of the various layer surfaces. The bump phase differences were integrated in the calculation in other works [59, 60].

The influence of this dipole coupling has already been observed in spin-valve systems [58, 61, 62] and MTJs [63]. Taking into account the small thickness in these structures, Néel coupling may reach values of the same order of magnitude as AF/F exchange anisotropy and is thus harmful to a good decoupling of the two ferromagnetic layers. Based on the experimental data and model analysis, the topological coupling, in a spin-valve type structure for example, could exceed 10 Oe even for fairly smooth interfaces ($\lambda/h \sim 100$) [56]. Depending on its strength, ferromagnetic coupling between the two layers may affect a TMR element in the following ways: (i) complete failure of the element; (ii) smaller field sensitivity and smaller TMR effect and (ii) unstable magnetic states, i.e., a loss of information stored in MRAM cells. Some recent studies [64] show the possibility of modifying the ferromagnetic orange-peel coupling in MTJs by an AF coupling to a third magnetic layer using the RKKY-like exchange coupling.

Influence of defects: biquadratic coupling. The biquadratic (second-order Heisenberg) coupling was introduced to explain the discrepancy between bilinear models and experimental magnetic behaviour in antiferromagnetically coupled multilayers [65]. Whereas antiferromagnetic coupling favours diametrically opposed spin moments, biquadratic coupling aligns spin moments perpendicular to each other.

In epitaxial Fe/Cr/Fe sandwiches Slonczewski [66, 67] interprets this 90° coupling as due to spatial fluctuations in the interlayer coupling through the Cr spacer caused by the presence of terraces at the Fe/Cr interfaces. That was experimentally checked by Purcell *et al* [68]. The biquadratic coupling is written as

$$B = \frac{4L(\Delta_J)^2}{\pi^3 A} \coth\left(\frac{\pi t}{L}\right) \tag{12}$$

where L is the terrace size, A the Fe stiffness constant, t the Fe thickness and Δ_J the difference of coupling between two terraces.

Independently of the sign fluctuation of the interlayer coupling, a general explanation of the biquadratic coupling is based on the pinhole model [69–71]. A pinhole is a ferromagnetic bridge between the two ferromagnetic layers caused by thickness discontinuities of the spacer. This direct exchange favours a parallel alignment of the magnetization. The density of pinholes is very dependent on growth conditions or crystalline orientation but it generally increases when decreasing the spacer thickness [72]. From a micromagnetic model and for given features of the ferromagnetic and non-magnetic layers (stiffness constant, thickness, ...), it is possible to find pinhole densities giving magnetization curves similar to those with biquadratic coupling.

Experimental determination of coupling. An AF coupling involves a magnetic period doubled with respect to the multilayer chemical period. The use of a magnetization-sensitive probe allows the description of the magnetic order. Two kinds of magnetic diffraction are available: neutron diffraction and resonant magnetic scattering in the soft x-ray range close to the absorption edge of the ferromagnetic element [73].

Encinas [74] presents in his thesis a method of determination of the coupling constant J in spin-valve structures or MTJs. This method is based on the measurement of minor loops of the soft layer assuming a perfect pinned magnetization of the hard layer. From the bilinear model, the coupling constant can be expressed as a function of the shift in field H_d of the minor cycle

$$J = -H_d M_s t. \tag{13}$$

M_s and t are respectively the saturation magnetization and the thickness of the soft layer.

3. Spin electronics

In this second part, we will review recent advances in spin electronics. Research in this field is very active and an increasing number of studies are being published in many physics journals. We will therefore restrict ourselves to a few topics in which major advances have recently been made, and whose relevance is great for the future of this field. The first part of this section will be dedicated to spin-polarized tunnelling, with special emphasis on the relevance of half-metallic ferromagnets, and the second part to magnetoresistance in nanostructures.

3.1. Spin-polarized tunnelling

3.1.1. Early experiments. In solid-state physics, tunnelling experiments are generally performed in trilayers consisting of two metallic electrodes sandwiching an insulating layer. In classical mechanics, no electrical current can flow from one electrode to the other due the presence of a potential barrier materialized by the insulator. However, if this insulating element is thin enough, there exists a probability that electrons may pass through it by a quantum mechanical effect called tunnelling. The thickness of the insulator must be in the range of a few tens of ångströms and it must form a continuous separation between the electrodes. These two conditions require a good control in thin film growth, and reliable tunnelling experiments were been performed until the 1960s. A model was proposed in 1963 by Simmons [75] to explain the observed behaviour of such trilayers, also called tunnel junctions. In this model, the tunnel current depends exponentially on the barrier thickness, and on the square root of its height. The model also accounts for the typical parabolic dependence of the conductance G of the junction on bias voltage V_{bias}, at intermediate values of V_{bias}.

This single-particle picture is however far too simple to explain all experiments, and especially those performed in normal metal–insulator–superconductor tunnel junctions. In such systems, the conductance remains zero for low voltage values, in contradiction to Simmons' model. Indeed, when tunnelling from a metal into a superconductor, there are no states available between E_F and $E_F + \Delta/2$ in the superconductor (Δ being the quasiparticle gap of the superconductor). Thus, tunnelling cannot occur until a voltage large enough to populate levels above the quasiparticle gap is applied. This is the first evidence for an influence of the DOS on the tunnelling process.

These studies were followed by a series of experiments performed by Meservey and Tedrow [76]. They focused on junctions between a ferromagnetic metal and a superconductor, and pioneered the field of spin-dependent tunnelling. The technique they developed allows us to determine the spin polarization P of the ferromagnet, $P = [N_\uparrow(E_F) - N_\downarrow(E_F)]/[N_\uparrow(E_F) + N_\downarrow(E_F)]$, $N(E_F)$ being the DOS at the Fermi energy. When a magnetic field is applied to the junction, the DOS in the superconductor is split by the Zeeman effect. Since the spin of the carriers involved in the tunnelling process is generally conserved, one can consider that spin-up and spin-down conduction electrons travel in two independent channels. Thus,

the conductance of the junction is the sum of that of both spin channels. In ferromagnetic metals, the number of spin-up and spin-down electrons participating in transport processes is not the same, and therefore the contribution of the two spin channels to the total conductance is weighted by the spin-up and spin-down DOS at the Fermi level, $N_\uparrow(E_F)$ and $N_\downarrow(E_F)$, in the ferromagnet. This results in an asymmetry in the conductance curves, compared to the case of junctions involving non-magnetic metals. By fitting these curves with an appropriate model, one can deduce the value of P.

3.1.2. Magnetic tunnel junctions. In 1975, a first result concerning tunnel junctions with two ferromagnetic electrodes was reported by Jullière [77], but it was only in 1995 that clear experimental evidence was provided by Moodera *et al* [78] through the observation of magnetoresistance cycles, see figure 10. Indeed, when electrons tunnel from one ferromagnet to another, the conductance is not the same if the magnetizations of the electrodes are aligned parallel or antiparallel. Assuming spin conservation in the tunnelling process, the total conductance in the parallel (P) and the antiparallel (AP) situations is written

$$G_P = G_{\uparrow\uparrow} + G_{\downarrow\downarrow} \tag{14}$$

$$G_{AP} = G_{\uparrow\downarrow} + G_{\uparrow\downarrow}. \tag{15}$$

Similar to the case of tunnelling between a ferromagnet and a superconductor, the contribution of both spin channels to the total conductance is proportional to the DOS at the Fermi energy. Here the DOS of both electrodes must be taken into account and thus $G_{\uparrow\uparrow(\downarrow)} \propto N_\uparrow(E_F)N_{\uparrow(\downarrow)}(E_F)$. Defining the tunnel magnetoresistance (TMR) as

$$\mathrm{TMR} = \frac{G_P - G_{AP}}{G_{AP}} = \frac{R_{AP} - R_P}{R_P} \tag{16}$$

we can relate it to the spin polarization of the electrodes. This is Jullière's formula:

$$\mathrm{TMR} = \frac{2P_1P_2}{1 - P_1P_2} \tag{17}$$

in which P_1 and P_2 are the spin polarizations of the two electrodes. When using values of P deduced from Meservey–Tedrow experiments, one can calculate the expected values of TMR for different systems. In junctions with electrodes made of transition metals (or their alloys) and Al_2O_3 barriers, a very good quantitative agreement is obtained. These compounds have spin-polarization values between 30 and 50%, leading to TMR ratios of up to about 65% at low temperature.

From equation (17), it is obvious that a natural way to increase the TMR is to use electrodes with large, ideally total, spin polarizations. This has motivated attempts to integrate half-metallic ferromagnets as electrodes in MTJs. These compounds show metallic conductance for one spin direction and have an insulating character for the other one. This can be due to the absence of states at E_F for this minority spin sub-band (thus, the Fermi level falls into a gap), or to the localization of charge carriers. In this case, the compound is called a 'transport half-metal' because only charges from one sub-band are mobile [79]. An increasing number of compounds are predicted to be half-metals. Many of them are oxides, such as mixed-valence manganites [80, 81], Fe_3O_4 [82], CrO_2 [83], $Tl_2Mn_2O_7$ [84] or some double perovskites (such as Sr_2FeMoO_6 [85]). Some full and half-Heusler alloys (such as as Mn_2VAl [86] and NiMnSb [87]), sulfospinels (such as $Fe_{1-x}Cu_xCr_2S_4$ [88]) and several binary compounds with zinc-blende structure [89] have also been predicted to have a total spin polarization. Some III–V semiconductors substituted with magnetic ions such as Mn or Co can also be considered as half-metallic ferromagnets, especially $Ga_{1-x}Mn_xAs$ [90]. Attempts have been made to confirm experimentally this half-metallic character, using spin-polarized photoemission spectroscopy,

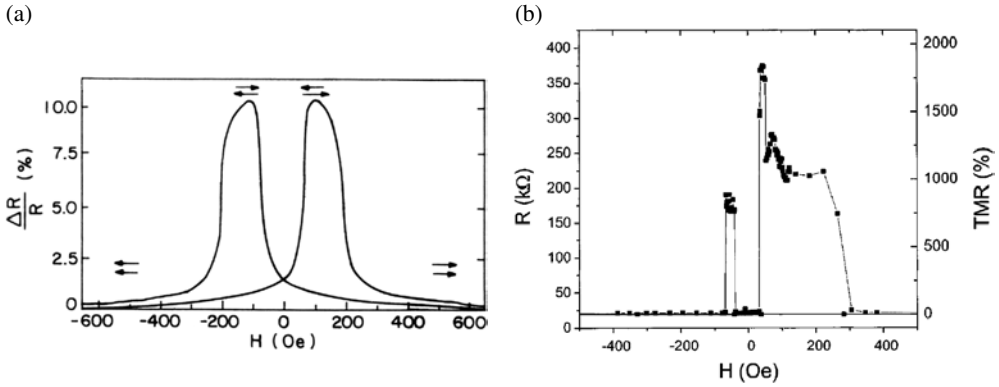

Figure 10. (a) First TMR result, obtained in a $CoFe/Al_2O_3/Co$ junction, at 295 K (adapted from [78]); (b) TMR cycle measured at 4.2 K in a $La_{2/3}Sr_{1/3}MnO_3/SrTiO_3/La_{2/3}Sr_{1/3}MnO_3$ junction [99].

Table 1. Properties of tunnel junctions integrating half-metals.

Structure of the junction	TMR (%)	$P_{\text{half-metal}}$ (%)	Reference
$CrO_2/Cr_2O_3/Co$	−7	8	[94]
$Fe_3O_4/Al_2O_3/Co$	43	42	[95]
$NiMnSb/Al_2O_3/Ni_{80}Fe_{20}$	19	19	[96]
$Sr_2FeMoO_6/SrTiO_3/Co$	50	−90	[97]
$La_{2/3}Ca_{1/3}MnO_3/NdGaO_3/La_{2/3}Ca_{1/3}MnO_3$	700	86	[98]
$La_{2/3}Sr_{1/3}MnO_3/SrTiO_3/La_{2/3}Sr_{1/3}MnO_3$	1850	95	[99]
$Ga_{0.96}Mn_{0.04}As/AlAs/Ga_{0.967}Sr_{0.033}As$	75	52	[100, 101]

Andreev reflection or the Meservey–Tedrow technique. So far, only CrO_2 [91, 92] and $La_{2/3}Sr_{1/3}MnO_3$ [93] have been shown to have a spin polarization larger than 95% by these techniques.

Among all these materials, only a few have been used as electrodes in MTJs, giving rise to a measurable TMR. These results are summarized in table 1. It is clear that only manganites lead to very large TMR ratios, as expected from their large spin polarization, within the Julliere model. The reasons for the low TMR values obtained in the other cases may be a non-optimal structural quality of the electrodes or some more intrinsic problem, e.g. a modification of the electronic structure at the interfaces with the barrier, producing a loss of the half-metallicity. This is still an open question but several groups are working on these systems and larger TMR might be reported in the near future.

We will now describe some transport properties of MTJs, starting with the dependence of their conductance and TMR on V_{bias}. Concerning the G versus V curves, if a parabolic variation is generally observed above about 150 mV, in agreement with Simmons' model, a deviation from this behaviour occurs at low bias ($|V_{\text{bias}}| \leqslant 150$ mV). This so-called zero-bias anomaly is a very general feature of MTJs with transition metal electrodes [102] but also of junctions with manganites [103–105]. Several models have been proposed to explain it, generally invoking inelastic scattering processes by magnons. The model of Zhang *et al* [106] proposes that the zero-bias anomaly is due to interfacial magnons excited by hot tunnelling electrons. Gu *et al* have developed a model [107] specific to double-exchange systems, such as manganites, which accounts at least qualitatively for the very specific shape of the zero-bias dip observed in manganite-based junctions [105].

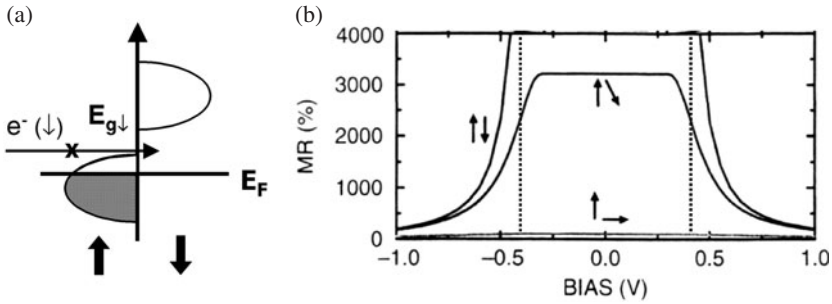

Figure 11. (a) Schematic representation of the electronic structure of a half-metallic ferromagnet. If this material is used as a collecting electrode in a tunnel junction, spin ↓ electrons with an energy $E < E_{g\downarrow}$ cannot tunnel because there are no states available for them at this energy. (b) Calculated bias dependence of the TMR between two identical half-metal ferromagnets with $E_{g\downarrow} = 0.4$ eV (adapted from [108]).

For bias voltages larger than 150 mV, this inelastic scattering effect saturates and other features can be observed. In particular, the influence of the DOS of the electrodes can strongly affect the G versus V_{bias} and TMR versus V_{bias} dependences. Bratovsky has developed a model predicting the bias dependence of the TMR in junctions with two half-metallic electrodes [108], see figure 11. Discarding inelastic scattering contributions, the TMR is found to be very large (in principle infinite) and constant at low bias since tunnelling is only allowed between the majority sub-bands of each electrode. When a bias large enough to populate levels of the bottom of the minority spin sub-band is applied, thus allowing tunnelling of minority-spin carriers, the TMR starts to decrease. This theoretical prediction has recently been confirmed experimentally by tunnelling experiments in LSMO/STO/LSMO junctions [99]. The bottom of the conduction band for ↓ spins is found to lie about 350 meV above E_F, which is in quantitative agreement with results from spin-polarized inverse photoemission spectroscopy measurements. Indications of the DOS signature in the TMR versus V_{bias} have also been found in junctions with a manganite bottom electrode and a counter-electrode based on transition metals. In this system, the spin-polarized tunnelling process probes the spin ↑ DOS of the barrier/counter-electrode interface in the parallel configuration, and the spin ↓ DOS of this interface in the antiparallel case. The strong energy dependence of the DOS of transition metals, due to the presence of d states close to or at the Fermi level, leads to a strong modulation of the conductances which is also reflected in the TMR versus V_{bias} dependence. These curves typically show a clear asymmetry, with sometimes a non-monotonic decrease when increasing bias. The first evidence for this behaviour was given by de Teresa *et al* [109] in the LSMO/STO/Co system. The TMR was -29% at low bias, with a maximum around -0.5 V, and a sign inversion above +0.6 V (for positive bias, electrons tunnel from Co to LSMO). Experiments with $Co_{90}Fe_{10}$ [110], $Co_{80}Fe_{20}$ and Fe [111] counter-electrodes have also been performed. Even though all the specific features observed by de Teresa *et al* on the LSMO/STO/Co system were not reported in these studies, the TMR versus V_{bias} were found to show clear signatures of DOS effects.

Aside from these results, the use of fully spin-polarized electrodes has also demonstrated that the properties of the tunnelling current are to a great extent determined by the electronic structure of the interfaces. Indeed, junctions with an LSMO bottom-electrode and a Co counter-electrode can either show a negative or positive TMR at low bias depending on whether STO or Al_2O_3 is used as a barrier [109], see figure 12. This arises from different bonding effects at the interface between Co and the barrier: when an alumina barrier is used, sp–d bonding would result in the preferential transmission of positively polarized sp states; alternatively, when the

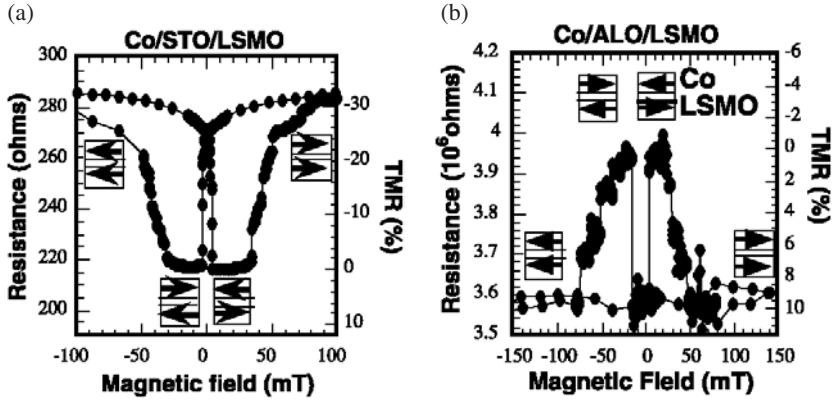

Figure 12. TMR cycles measured at 4.2 K for LSMO/TiO_2/Co (a) and LSMO/Al_2O_3 junctions [109] (b).

barrier is STO, d–d bonding leads to the transmission of d states with negative polarization. Both the Al_2O_2/Co and $SrTiO_3$/Co interfaces have been studied theoretically by Oleinik *et al* [112, 113]. In the case of STO, the negative spin polarization of the tunnel current is found to arise from a magnetic moment induced on the Ti atoms of the interface. This has not been confirmed by experiments so far [114]. For alumina, the spin polarization is found to be negative just at the interface, but the decay length of ↑ states inside the barrier is shorter than that of ↓ states, which results in a cross-over from negative to positive effective spin polarization when increasing the barrier thickness (at about 10 Å). This picture is in agreement with the experimental results of [109].

Some other interesting experiments aiming at understanding the role of interfaces in the tunnelling process have been reported by LeClair *et al*. These studies do not involve half-metallic electrodes and therefore cannot benefit from the advantage of a fully spin-polarized source of electrons. However, by introducing a small amount of non-ferromagnetic material ('dusting'), such as Cu [115] or Cr [116], at the interface between one electrode and the barrier in Co/Al_2O_3/Co junctions, it is possible to analyse the relevance of the interfaces' structural and electronic properties. A general feature of these data is an exponential decay of the TMR upon increasing the amount of dusting material. In the case of Cu dusting, the decay length is 2.8 Å if Cu is introduced at the interface between the bottom Co electrode and the barrier, and 6.2 Å when Cu is introduced above the barrier. These very small values clearly illustrate the interfacial character of the tunnel process: the properties of the very first monolayers near the electrode–barrier interface completely dictate the value of the TMR. The difference between these two decay lengths (for bottom dusting and top dusting) is attributed to different growth mechanisms for Cu on top of Co and Al_2O_3. For Cr dusting, the situation is similar, i.e. the TMR decays quickly with the amount of dusting material.

3.2. Magnetoresistance in nanostructures

In the last three years, there has been an increasing interest in magnetoresistance phenomena in magnetic nanostructures. Beside the fundamental interest in spin-dependent transport in the ballistic regime, this interest was to a great extent motivated by the report of a 280% MR at room temperature and a field of 20 Oe in a nanocontact between two Ni wires by García *et al* [117]; see figure 13(a). This was followed by reports of MR in Fe and Co nanocontacts created by the same technique. In these experiments, electron transport is ballistic since the length

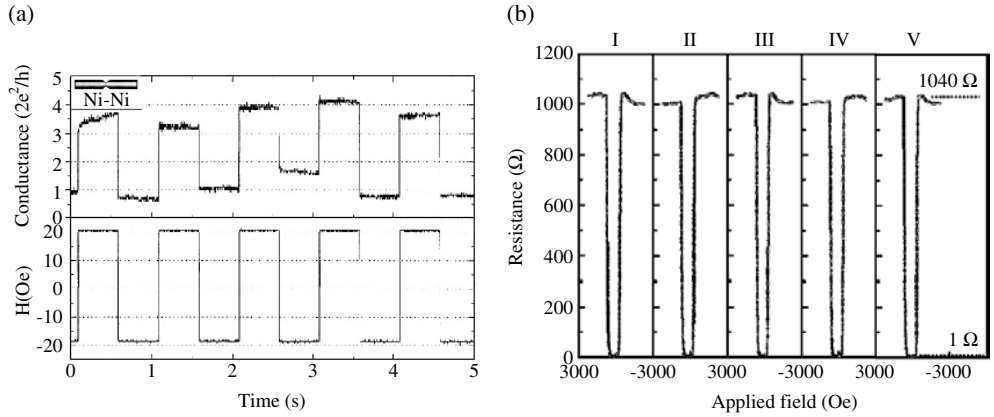

Figure 13. (a) Magnetic field response of a nanocontact between two macroscopic Ni wires (from [117]). (b) Successive MR versus H loops obtained in an electrodeposited Ni contact [118].

of the contact is smaller than the mean free path, and the conductance usually stabilizes near integer multiples of the conductance quantum $G_0 = 2e^2/\hbar$, which evidences the very small size of these contacts. Both the very large value of the MR and these very reduced dimensions make such nanostructures possible candidates for future memory elements with densities in the Tbits/square inch range.

A possible explanation for this magnetoresistive effect is DW scattering [119]. Indeed, if DW scattering leads to a negligible magnetoresistance in bulk materials where the DW width is of the order of several tens of nanometres, it may produce large effects in very thin walls. If the DW width is large enough for an electron to have its spin always aligned with the local magnetization, the wall will be transparent and zero MR will result. Alternatively, if the wall becomes very thin, the electron spin might not follow the rotation of the local magnetization on its travel across the DW, which will result in a resistivity increase, and thus in a magnetoresistance. Within this framework, it is natural to expect that MR will increase when decreasing the DW width. Since the typical DW width in bulk materials does not lead to any MR, it is a challenge to design structures in which DW widths could be reduced and lead to large MR values. As was shown by Bruno [120], this can be done by creating narrow constrictions in a magnetic sample. The minimization of the total wall energy would in principle be achieved by locating the DWs inside the constrictions. The DW width would then be approximately equal to the curvature radius on the constriction and, if the constriction is narrow enough, would thus fulfil the requisite for obtaining substantial MR ratios. This mechanism was proposed to explain the very large MR obtained by García *et al* [121, 122]. In particular, a general decay of the MR upon increasing the size of the nanocontact (monitored by the increase of the conductance) was observed.

Other techniques have been used to produce very small contacts. In break-junctions (created by approaching the two parts of a bridge or a wire previously broken by stretching) of Ni, Viret and co-workers [123], although working with a very similar configuration to that of García *et al*, only observed an MR of about 40% (at low temperature). However, break-junctions of $La_{2/3}Sr_{1/3}MnO_3$ have yielded an MR of more than 500% at room temperature, an unprecedented result for this compound [124].

More recently, small contacts have been obtained by electrodepositing Ni between two Ni tips. Several groups have reported very large MR [125–128] (see figure 13(b)), with a record value of 100 000% [118]. In these systems, the contact is larger than 10 nm and thus DW

scattering cannot account for the magnetoresistive effect. A possible explanation is that a dead layer about 1 nm thick forms just at the contact, due to the electrodeposition process, and acts as the non-magnetic spacer of a CCP GMR trilayer [129]. Another possibility is that some oxygen ions are trapped just at the contact. According to electronic structure calculations [130], Ni ions would induce a very large local spin polarization to the oxygen, which would therefore be responsible for these very large MR ratios. These two possible explanations are only speculations and systematic experiments are certainly required to understand the physics behind these promising effects.

4. Conclusion

We have tried to give in this paper an overview of the physics of magnetic nanostructures and spin electronics based on ultrathin films and nanostructures. These effects, when they are combined, yield systems that can be named *nanomagnetoelectronic* components. These devices may lead to an exciting new generation of applications. However, important efforts are still required, by fundamental material science researchers as well as by device developers, to achieve them. We hope that this review helps in this way.

Acknowledgments

The authors would like to thank Professors P Bruno, A Fert and A R Fert and Dr C Chappert for fruitful lectures or discussions that helped in writing this paper. Help from the authors who contributed to this paper by giving us materials for several figures is also acknowledged. We also thank Professor E Burkel who organized Euroschool in Rostock[3] for giving us the opportunity to publish this paper.

References

[1] Kittel C 1976 *Introduction to Solid State Physics* (New York: Wiley) chapter 15
[2] Fert A 1990 Magnetic and transport properties of metallic multilayers *Mater. Sci. Forum* **59/60** 439
[3] Bruno P 1991 *Magnetic Surfaces, Thin Films, and Multilayers Symp.* (Pittsburgh, PA: Materials Research Society) p 299
[4] Piecuch M, Andrieu S, Bobo J F, Maurer M, Ravet M F, Dupuis V, Ousset J C and Dieny B 1991 *Proc. 1991 MRS Spring Mtg* (*Materials Research Society Proc.* vol 232) (Pittsburgh, PA: Materials Research Society) p 165
[5] Andrieu S, Piecuch M and Bobo J F 1992 *Phys. Rev.* B **46** 4909
[6] Bergter E, Gradmann U and Bergholz R 1985 *Solid State Commun.* **53** 565
[7] Gradmann U and Müler J 1968 *Phys. Status Solidi* **27** 313
[8] Draaisma H G J, De Jonge W M J and Den Broeder F J A 1987 *J. Magn. Magn. Mater.* **66** 351
[9] Liu C, Moog E R and Bader S D 1988 *Phys. Rev. Lett.* **60** 23
[10] Pratzer M, Elmers H J, Bode M, Pietzsch O, Kubetzka A and Wiesendanger R 2001 *Phys. Rev. Lett.* **87** 127201
[11] Pratzer M and Elmers H J 2002 *Phys. Rev.* B **66** 033402
[12] Dubourg S, Bobo J F, Warot B, Snoeck E and Ousset J C 2001 *Phys. Rev.* B **64** 054416
[13] Bobo J F *et al* 2003 *ICM Proc.*; *J. Magn. Magn. Mater.* at press
[14] Sugawara A, Hembree G G and Scheinfein M R 1997 *J. Appl. Phys.* **82** 5662
[15] Martín J I, Nogués J, Liu K, Vicent J L and Schuller I K 2003 *J. Magn. Magn. Mater.* **256** 449
[16] Cowburn R P and Welland M E 2000 *Science* **287** 1466
[17] Cowburn R P and Welland M E 2000 *J. Appl. Phys.* **88** 5315
[18] Cowburn R P 2002 *Phys. Rev.* B **65** 092409
[19] Cowburn R P 2002 *J. Magn. Magn. Mater.* **242–245** 505

[3] Euroschool is supported by the European Community; its website is http://euroschool.physik.uni-rostock.de

[20] Hrabovský D, Ciprian D, Jaworowicz J, Gmitra M, Horvarth D, Vavra I, Fert A R and Pistora J 2002 *Trans. Magn. Soc. Japan* **2** 240
[21] Hyndman R, Warin P, Gierak J, Ferré J, Chapman J N, Jamet J P, Mathet V and Chappert C 2001 *J. Appl. Phys.* **90** 3843
[22] Warin P, Hyndman R, Gierak J, Chapman J N, Ferré J, Jamet J P, Mathet V and Chappert C 2001 *J. Appl. Phys.* **90** 3850
[23] Hyndman R, Mougin A, Repain V, Ferré J, Jamet J P, Gierak J, Mailly D, Chappert C, Mathet V, Warin P and Chapman J N 2002 *Trans. Magn. Soc. Japan* **2** 175
[24] Hyndman R, Mougin A, Sampaio L C, Ferré J, Jamet J P, Meyer P, Mathet V, Chappert C, Mailly D and Gierak J 2002 *J. Magn. Magn. Mater.* **240** 34
[25] Meiklejohn W H and Bean C P 1956 *Phys. Rev.* **102** 1413
Meiklejohn W H and Bean C P 1957 *Phys. Rev.* **105** 904
[26] Meiklejohn W H and Bean C P 1957 *Phys. Rev.* **105** 904
[27] Bean C P 1959 *Structure and Properties of Thin Films* (New York: Wiley) p 331
[28] Meiklejohn W H 1962 *J. Appl. Phys.* **33** 1328
[29] Nogués J, Moran T J, Lederman D and Schuller I K 1999 *Phys. Rev.* B **59** 6984
[30] Ohldag H, Scholl A, Nolting F, Anders S, Hillebrecht F U and Stöhr J 2001 *Phys. Rev. Lett.* **86** 2878
[31] Ohldag H 2003 unpublished
[32] Dubourg S, Bobo J F, Ousset J C, Warot B and Snoeck E 2002 *J. Appl. Phys.* **91** 7757
[33] Hrabovský D, Diouf B, Gabillet L, Fert A R and Bobo J F 2003 unpublished
[34] Nogués J, Lederman D, Moran T J and Schuller I K 1996 *Phys. Rev. Lett.* **76** 4624
[35] Nogués J and Schuller I K 1997 unpublished
[36] Diouf B, Gabillet L, Fert A R, Hrabovský D, Prochazka V, Snoeck E and Bobo J F 2003 *J. Magn. Magn. Mater.* **265/2** 204
[37] Nogués J, Sort J, Suriñach S, Muñoz J S, Baró M D, Bobo J F, Lüders U, Haanapel E, Fitzsimmons M R, Hoffmann A and Cai J W 2003 *Appl. Phys. Lett.* **82** 3044
[38] Nogués J and Schuller I K 1999 *J. Magn. Magn. Mater.* **192** 203
[39] Grünberg P, Shreiber R, Pang Y, Brodsky M B and Sowers H 1986 *Phys. Rev. Lett.* **57** 2442
[40] Carbone C *et al* 1987 *Phys. Rev.* B
[41] Majkrzak C F, Cable J W, Kwo J, Hong M, McWhan D B, Yafet Y, Waszcak J V and Vettier C 1986 *Phys. Rev. Lett.* **56** 2700
[42] Salomon M B, Sinha S, Rhyne J J, Cunningham J E, Erwin R W, Borchers J and Flynn C P 1986 *Phys. Rev. Lett.* **56** 259
[43] Baibich M N, Broto J M, Fert A, Nguyen Van Dau F, Petroff F, Etienne P, Creuzet G, Friederich A and Chazelas J 1988 *Phys. Rev. Lett.* **61** 2472
[44] Parkin S S P 1991 *Phys. Rev. Lett.* **67** 3598
[45] Ruderman M A and Kittel C 1954 *Phys. Rev.* **96** 99
[46] Bobo J F *et al* 1993 *J. Magn. Magn. Mater.* **126** 251
[47] Chappert C and Renard J P 1991 *Europhys. Lett.* **15** 553
[48] Coehoorn R 1991 *Phys. Rev.* B **44** 9331
[49] Bruno P and Chappert C 1991 *Phys. Rev. Lett.* **67** 1602
Bruno P and Chappert C 1991 *Phys. Rev. Lett.* E **67** 2592
Bruno P and Chappert C 1992 *Phys. Rev.* B **46** 261
[50] Johnson M T, Purcell S T, McGee N W E, Coehoorn R, aan de Stegge J and Hoving W 1992 *Phys. Rev. Lett.* **68** 2688
[51] Johnson M T, Coehoorn R, de Vries J J, McGee N W E, aan de Stegge J and Bloemen P J H 1992 *Phys. Rev. Lett.* **69** 969
[52] Bruno P 1993 *Europhys. Lett.* **23** 615
[53] Stiles M D 1999 *J. Magn. Magn. Mater.* **200** 322
[54] Néel L 1966 *C. R. Acad. Sci.* **255** 1545
[55] Néel L 1966 *C. R. Acad. Sci.* **255** 1676
[56] Zhang J and White R M 1996 *IEEE* **32** 4630
[57] Kools J C S 1996 *IEEE* **32** 3165
[58] Kools J C S, Kula W, Mauri D and Lin T 1999 *J. Appl. Phys.* **85** 4466
[59] Yang J, Lee J and Chang C 1998 *IEEE* **34** 2469
[60] Chang C and Yang J 1996 *IEEE* **32** 714
[61] Chopra H D, Yang D X, Chen P J, Parks D C and Egelhoff W F Jr 2000 *Phys. Rev.* B **61** 9642
[62] Kim K Y, Jang S H, Shin K H, Kim H J and Kang T 2001 *J. Appl. Phys.* **89** 7612

[63] Tegen S, Mönch I, Schuman J, Vinzelberg H and Schneider C M 2001 *J. Appl. Phys.* **89** 8169
[64] Luncinski T, Brückl H, Justus M, Hütten A and Reiss G 2002 *J. Magn. Magn. Mater.* **239** 138
[65] Rührig M, Schäfer R, Hubert A, Mosler R, Wolf J A, Demokritov S and Grünberg P 1991 *Phys. Status Solidi* a 635
[66] Slonczewski J C 1991 *Phys. Rev. Lett.* **67** 3172
[67] Slonczewski J C 1993 *J. Appl. Phys.* **73** 5957
[68] Purcell S T, Folkerts W, Johnson M T, McGee N W E, Jager K, aan de Stegge J, Zeper W B and Hoving W 1991 *Phys. Rev. Lett.* **67** 3172
[69] Bobo J F, Fischer H and Piecuch M 1993 *Mater. Res. Soc. Symp. Proc.* **313** 467
Bobo J F, Snoeck E, Piecuch M and Casanove M J 1994 *Mater. Res. Soc. Symp. Proc.* **343** 423
[70] Bobo J F, Kikuchi H, Redon O, Snoeck E, Piecuch M and White R L 1999 *Phys. Rev.* B **60** 4131
[71] Fulghum D B and Camley R E 1995 *Phys. Rev.* B **52** 13436
[72] Dieny B 1994 *J. Magn. Magn. Mater.* **136** 355
[73] Sève L, Tonnerre J M, Raoux D, Bobo J F, Piecuch M, De Santis M, Troussel P, Brot J M, Chakarian V, Kao C C and Chen C T 1995 *J. Magn. Magn. Mater.* **148** 68
[74] Encinas A 1999 *Thesis* University Paris Sud, Orsay
[75] Simmons J G 1963 *J. Appl. Phys.* **34** 1763
[76] Tedrow P M and Meservey R 1994 *Phys. Rep.* **238** 173
[77] Jullière M 1975 *Phys. Lett.* A **54** 225
[78] Moodera J S, Kinder L R, Wong T M and Meservey R 1995 *Phys. Rev. Lett.* **74** 3273
[79] Coey J M D and Venkatesan M 2002 *J. Appl. Phys.* **91** 8345
[80] Pickett W E and Singh D J 1996 *Phys. Rev.* B **53** 1146
[81] Coey J M D, Viret M and von Molnär S 1999 *Adv. Phys.* **48** 167
[82] Penicaud M, Silberchiot B, Sommers C B and Kubler J 1992 *J. Magn. Magn. Mater.* **103** 212
[83] Lewis S P, Allen P B and Sasaki T 1997 *Phys. Rev.* B **55** 10253
[84] Singh D J 1997 *Phys. Rev.* B **55** 313
[85] Kobayashi K I, Kimura T, Sawada H, Terakura K and Tokura Y 1998 *Nature* **395** 677
[86] Weht E and Pickett W E 1999 *Phys. Rev.* B **60** 13006
[87] de Groot R A, Mueller F M, van Engen P G and Buschow K H J 1983 *Phys. Rev. Lett.* **50** 2024
[88] Park M S, Kwon S K, Youn S J and Min B I 1999 *Phys. Rev.* B **59** 10018
[89] Galanakis I and Mavropoulos P 2002 *Preprint* condmat/0209039
[90] Sanvito S, Ordejón P and Hill N A 2001 *Phys. Rev.* B **63** 165206
[91] Soulen R J, Byers J M, Osofsky M S, Nadgorny B, Ambrose T, Cheng S F, Broussard P R, Tanaka C T, Nowak J, Moodera J S, Barry A and Coey J M D 1998 *Science* **282** 85
[92] Parker J S, Watts S M, Ivanov P G and Xiong P 2002 *Phys. Rev. Lett.* **88** 196601
[93] Park J H, Vescovo E, Kim H J, Kwon C, Ramesh R and Venkatesan T 1998 *Nature* **392** 794
[94] Gupta A, Li X W and Xiao G 2001 *Appl. Phys. Lett.* **78** 1894
[95] Seneor P, Fert A, Maurice J-L, Montaigne F, Petroff F and Vaurès A 1999 *Appl. Phys. Lett.* **74** 4017
[96] Tanaka H *et al* 1999 *J. Appl. Phys.*
[97] Bibes M, Bouzehouane K, Besse M, Barthélémy A, Fusil S, Bowen M, Seneor P, Contour J P and Fert A 2003 *Appl. Phys. Lett.* **83** 2629
[98] Jo M H, Mathur N D, Todd N K and Blamire M 2000 *Phys. Rev.* B **61** R14905
[99] Bowen M, Bibes M, Barthélémy A, Contour J P, Anane A, Lemaître Y and Fert A 2003 *Appl. Phys. Lett.* **82** 233
[100] Higo Y, Shimizu H and Tanaka M 2001 *J. Appl. Phys.* **89** 6745
[101] Tanaka M and Higo Y 2001 *Phys. Rev. Lett.* **87** 026602
[102] Han X F, Yu A C C, Oogane M, Murai J, Daibou T and Miyazaki T 2001 *Phys. Rev.* B **63** 224404
[103] Lu Y, Li W, Gong G Q, Xiao G, Gupta A, Lecoeur P, Sun J Z, Wang Y Y and Dravid V P 1996 *Phys. Rev.* B **54** R8357
[104] O'Donnell J, Eckstein J N and Rzchowski M S 2000 *Appl. Phys. Lett.* **76** 218
[105] Bibes M *et al* 2003 unpublished
[106] Zhang S, Levy P M, Marley A C and Parkin S S P 1997 *Phys. Rev. Lett.* **79** 3744
[107] Gu R Y, Sheng L and Ting C S 2001 *Phys. Rev.* B **63** 220406
[108] Bratkovsky A M 1997 *Phys. Rev.* B **56** 2344
[109] de Teresa J M, Barthélémy A, Fert A, Contour J P, Montaigne F and Seneor P 1999 *Science* **286** 507
[110] Hayakama J, Kokado S, Ito K, Sugiyama M, Asano H, Matsui M, Sakuma A and Ichimura M 2002 *Japan. J. Appl. Phys.* **41** 1340
[111] Sun J Z, Roche K P and Parkin S S P 2000 *Phys. Rev.* B **61** 11244

[112] Oleinik I I, Tsymbal E Y and Pettifor D G 2000 *Phys. Rev.* B **62** 3952
[113] Oleinik I I, Tsymbal E Y and Pettifor D G 2001 *Phys. Rev.* B **65** 020401
[114] Petroff F *et al* 2003 unpublished
[115] LeClair P, Swagten H J M, Kohlhepp J T, van de Veerdonk R J M and de Jonge W J M 2000 *Phys. Rev. Lett.* **84** 2933
[116] LeClair P, Kohlhepp J T, Swagten H J M and de Jonge W J M 2001 *Phys. Rev. Lett.* **86** 1066
[117] García N, Muñoz M and Zhao Y W 1999 *Phys. Rev. Lett.* **82** 2923
[118] Hua S Z and Chopra H D 2003 *Phys. Rev.* B **67** 60401-1–4
[119] Cabrera G C and Falicov L M 1974 *Phys. Status Solidi* b **61** 539
[120] Bruno P 1999 *Phys. Rev. Lett.* **83** 2425
[121] Tatara G, Zhao Y W, Muñoz M and García N 1999 *Phys. Rev. Lett.* **83** 2030
[122] Chung S H, Muñoz M, García N, Egelhoff W F and Gomez R D 2002 *Phys. Rev. Lett.* **89** 287203
[123] Viret M, Berger S, Gabureac M, Olligs D, Petej I, Gregg J F, Ott F, Francinet G, LeGoff G and Fermon C 2002 *Phys. Rev.* B **66** 220401
[124] Baszynski J and Tolinski T 2000 *Acta Phys. Pol.* A **98** 567
[125] García N, Muñoz M, Qian G G, Rohrer H, Saveliev I G and Zhao Y W 2001 *Phys. Rev. Lett.* **87** 026601
[126] Chopra H D and Hua S Z 2002 *Phys. Rev. Lett.* **66** 020403
[127] Piraux L 2002 private communication
[128] Wang H, Cheng H and García N 2002 *Preprint* cond-mat/0204516
[129] Barthélélemy A, Petroff F and Fert A 2002 *Handbook of Magnetic Materials* vol 12, ed K Buschow (Amsterdam: North-Holland)
[130] Papanikolaou N 2002 *Preprint* cond-mat/0210551